# IMPRS Ultrafast Source Technology

Franz X. Kaertner /Uemit Demirbas

SoSe 2017

# Chapter 2

# Classical Optics

The classical electromagnetic phenomena are completely described by Maxwell's Equations. The simplest case we may consider is that of electrodynamics of isotropic media

## 2.1 Maxwell's Equations and Helmholtz Equation

Maxwell's Equations are

$$\nabla \times \vec{H} = \frac{\partial \vec{D}}{\partial t} + \vec{J}, \tag{2.1a}$$

$$\nabla \times \vec{E} = -\frac{\partial \vec{B}}{\partial t}, \tag{2.1b}$$

$$\nabla \cdot \vec{D} = \rho, \tag{2.1c}$$

$$\nabla \cdot \vec{B} = 0. \tag{2.1d}$$

The material equations accompanying Maxwell's equations are:

$$\vec{D} = \epsilon_0 \vec{E} + \vec{P}, \tag{2.2a}$$

$$\vec{B} = \mu_0 \vec{H} + \vec{M}. \tag{2.2b}$$

Here, $\vec{E}$ and $\vec{H}$ are the electric and magnetic field strength, $\vec{D}$ the electric flux density, $\vec{B}$ the magnetic flux density, $\vec{J}$ the current density of free charges, $\rho$ is the free charge density, $\vec{P}$ is the polarization, and $\vec{M}$ the magnetization.

Note, it is Eqs.(2.2a) and (2.2b) which make electromagnetism an interesting and always a hot topic with never ending possibilities. All advances in engineering of artifical materials or finding of new material properties, such as superconductivity and meta-materials, bring new life, meaning and possibilities into this field.

By taking the curl of Eq. (2.1b) and considering

$$\nabla\times\left(\nabla\times\vec{E}\right)=\nabla\left(\nabla\cdot\vec{E}\right)-\Delta\vec{E},$$

where $\nabla$ is the Nabla operator and $\Delta$ the Laplace operator, we obtain

$$\Delta\vec{E}-\mu_0\frac{\partial}{\partial t}\left(\vec{j}+\epsilon_0\frac{\partial\vec{E}}{\partial t}+\frac{\partial\vec{P}}{\partial t}\right)=\frac{\partial}{\partial t}\nabla\times\vec{M}+\nabla\left(\nabla\cdot\vec{E}\right) \tag{2.3}$$

and hence

$$\left(\Delta-\frac{1}{c_0^2}\frac{\partial^2}{\partial t^2}\right)\vec{E}=\mu_0\left(\frac{\partial\vec{j}}{\partial t}+\frac{\partial^2}{\partial t^2}\vec{P}\right)+\frac{\partial}{\partial t}\nabla\times\vec{M}+\nabla\left(\nabla\cdot\vec{E}\right). \tag{2.4}$$

with the vacuum velocity of light

$$c_0=\sqrt{\frac{1}{\mu_0\epsilon_0}}. \tag{2.5}$$

For dielectric non magnetic media, which we often encounter in optics, with no free charges and currents due to free charges, there is $\vec{M}=\vec{0}$, $\vec{J}=\vec{0}$, $\rho=0$. One can also show that the electric field can be decomposed into a longitudinal and tranasversal component $\vec{E}_L$ and $\vec{E}_T$, which are characterized by [6]

$$\vec{\nabla}\times\vec{E}_L=0 \text{ and } \vec{\nabla}\cdot\vec{E}_T=0 \tag{2.6}$$

If there are no free charges, the longitudinal component is zero and only a transversal component is left over. Therefore, for the purpose of this class (and most of optics) the wave equation greatly simplifies to

$$\left(\Delta-\frac{1}{c_0^2}\frac{\partial^2}{\partial t^2}\right)\vec{E}=\mu_0\frac{\partial^2}{\partial t^2}\vec{P}. \tag{2.7}$$

This is the wave equation driven by the polarization of the medium in which the field propagates.

### 2.1.1 Helmholtz Equation

In general, the polarization in dielectric media may have a nonlinear and non local dependence on the field. For linear media the polarizability of the medium is described by a dielectric susceptibility $\chi(\vec{r},t)$

$$\vec{P}(\vec{r},t) = \epsilon_0 \int\int d\vec{r}'dt' \; \chi(\vec{r}-\vec{r}',t-t')\,\vec{E}(\vec{r}',t'). \tag{2.8}$$

The polarization in media with a local dielectric suszeptibility can be described by

$$\vec{P}(\vec{r},t) = \epsilon_0 \int dt' \; \chi(\vec{r},t-t')\,\vec{E}(\vec{r},t'). \tag{2.9}$$

This relationship further simplifies for homogeneous media, where the susceptibility does not depend on location

$$\vec{P}(\vec{r},t) = \epsilon_0 \int dt' \; \chi(t-t')\,\vec{E}(\vec{r},t'). \tag{2.10}$$

which leads to a dielectric response function or permittivity

$$\epsilon(t) = \epsilon_0(\delta(t)+\chi(t)) \tag{2.11}$$

and with it to

$$\vec{D}(\vec{r},t) = \int dt' \; \epsilon(t-t')\,\vec{E}(\vec{r},t'). \tag{2.12}$$

If the medium is linear and has only an induced polarization, completely described in the time domain $\chi(t)$ or in the frequency domain by its Fourier transform, the complex susceptibility $\tilde{\chi}(\omega) = \tilde{\epsilon}_r(\omega) - 1$ with the relative permittivity $\tilde{\epsilon}_r(\omega) = \tilde{\epsilon}(\omega)/\epsilon_0$, we obtain in the frequency domain with the Fourier transform relationship

$$\widetilde{\vec{E}}(\vec{r},\omega) = \int_{-\infty}^{+\infty} \vec{E}(\vec{r},t)e^{-j\omega t}dt, \tag{2.13}$$

$$\widetilde{\vec{P}}(\vec{r},\omega) = \epsilon_0\tilde{\chi}(\omega)\widetilde{\vec{E}}(\vec{r},\omega), \tag{2.14}$$

where, the tildes denote the Fourier transforms in the following. Substituted into (2.7)

$$\left(\Delta + \frac{\omega^2}{c_0^2}\right)\widetilde{\vec{E}}(\vec{r},\omega) = -\omega^2\mu_0\epsilon_0\tilde{\chi}(\omega)\widetilde{\vec{E}}(\vec{r},\omega), \tag{2.15}$$

we obtain

$$\left(\Delta + \frac{\omega^2}{c_0^2}(1+\tilde{\chi}(\omega)\right)\widetilde{\vec{E}}(\vec{r},\omega) = 0, \tag{2.16}$$

with the refractive index $n(\omega)$ and $1+\tilde{\chi}(\omega) = \tilde{n}(\omega)^2$ results in the Helmholtz equation

$$\left(\Delta + \frac{\omega^2}{c^2}\right)\widetilde{\vec{E}}(\vec{r},\omega) = 0, \tag{2.17}$$

where $c(\omega) = c_0/\tilde{n}(\omega)$ is the velocity of light in the medium. This equation is the starting point for finding monochromatic wave solutions to Maxwell's equations in linear media, as we will study for different cases in the following. So far we have treated the susceptibility $\tilde{\chi}(\omega)$ as a real quantity, which may not always be the case as we will see later in detail.

### 2.1.2 Plane-Wave Solutions (TEM-Waves) and Complex Notation

The real wave equation (2.7) for a linear medium has real monochromatic plane wave solutions $\vec{E}_{\vec{k}}(\vec{r},t)$, which can be be written most efficiently in terms of the complex plane-wave solutions $\underline{\vec{E}}_{\vec{k}}(\vec{r},t)$ according to

$$\vec{E}_{\vec{k}}(\vec{r},t) = \frac{1}{2}\left[\underline{\vec{E}}_{\vec{k}}(\vec{r},t) + \underline{\vec{E}}_{\vec{k}}(\vec{r},t)^*\right] = \Re e\left\{\underline{\vec{E}}_{\vec{k}}(\vec{r},t)\right\}, \tag{2.18}$$

with

$$\underline{\vec{E}}_{\vec{k}}(\vec{r},t) = \underline{E}_{\vec{k}}\; e^{\mathrm{j}(\omega t - \vec{k}\cdot\vec{r})}\; \vec{e}(\vec{k}). \tag{2.19}$$

Note, we explicitly underlined the complex wave to indicate that this is a complex quantity. Here, $\vec{e}(\vec{k})$ is a unit vector indicating the direction of the electric field which is also called the polarization of the wave, and $\underline{E}_{\vec{k}}$ is the complex field amplitude of the wave with wave vector $\vec{k}$. Substitution of eq.(2.18) into the wave equation results in the dispersion relation, i.e. a relationship between wave vector and frequency necessary to satisfy the wave equation

$$|\vec{k}|^2 = \frac{\omega^2}{c(\omega)^2} = k(\omega)^2. \tag{2.20}$$

The relation between wave vector and frequency of a wave is called dispersion relation. Here, it is given by

$$k(\omega) = \pm\frac{\omega}{c_0}n(\omega). \tag{2.21}$$

with the wavenumber

$$k = 2\pi/\lambda, \tag{2.22}$$

where $\lambda$ is the wavelength of the wave in the medium with refractive index $n$, $\omega$ the angular frequency, $\vec{k}$ the wave vector. Note, the natural frequency $f = \omega/2\pi$. From $\nabla \cdot \vec{E} = 0$, for all time, we see that $\vec{k} \perp \vec{e}$. Substitution of the electric field 2.18 into Maxwell's Eqs. (2.1b) results in the magnetic field

$$\vec{H}_{\vec{k}}(\vec{r}, t) = \frac{1}{2}\left[\underline{\vec{H}}_{\vec{k}}(\vec{r}, t) + \underline{\vec{H}}_{\vec{k}}(\vec{r}, t)^*\right] \tag{2.23}$$

with

$$\underline{\vec{H}}_{\vec{k}}(\vec{r}, t) = \underline{H}_{\vec{k}}\ e^{\mathrm{j}(\omega t - \vec{k}\cdot\vec{r})}\ \vec{h}(\vec{k}). \tag{2.24}$$

This complex component of the magnetic field can be determined from the corresponding complex electric field component using Faraday's law

$$-\mathrm{j}\vec{k} \times \left(\underline{E}_{\vec{k}}\ e^{\mathrm{j}(\omega t - \vec{k}\cdot\vec{r})}\ \vec{e}(\vec{k})\right) = -\mathrm{j}\mu_0\omega\underline{\vec{H}}_{\vec{k}}(\vec{r}, t), \tag{2.25}$$

or

$$\underline{\vec{H}}_{\vec{k}}(\vec{r}, t) = \frac{\underline{E}_{\vec{k}}}{\mu_0\omega}e^{\mathrm{j}(\omega t - \vec{k}\cdot\vec{r})}\vec{k} \times \vec{e} = \underline{H}_{\vec{k}}e^{\mathrm{j}(\omega t - \vec{k}\cdot\vec{r})}\vec{h} \tag{2.26}$$

with

$$\vec{h}(\vec{k}) = \frac{\vec{k}}{|k|} \times \vec{e}(\vec{k}) \tag{2.27}$$

and

$$\underline{H}_{\vec{k}} = \frac{|k|}{\mu_0\omega}\underline{E}_{\vec{k}} = \frac{1}{Z_F}\underline{E}_{\vec{k}}. \tag{2.28}$$

The characteristic impedance of the TEM-wave is the ratio between electric and magnetic field strength

$$Z_F = \mu_0 c = \sqrt{\frac{\mu_0}{\epsilon_0\epsilon_r}} = \frac{1}{n}Z_{F_0} \tag{2.29}$$

with the refractive index $n = \sqrt{\epsilon_r}$ and the free space impedance

$$Z_{F_0} = \sqrt{\frac{\mu_0}{\epsilon_0}} \approx 377\,\Omega. \tag{2.30}$$

Note that the vectors $\vec{e}$, $\vec{h}$ and $\vec{k}$ form an orthogonal trihedral,

$$\vec{e} \perp \vec{h}, \quad \vec{k} \perp \vec{e}, \quad \vec{k} \perp \vec{h}. \tag{2.31}$$

That is why we call these waves transverse electromagnetic (TEM) waves. We consider the electric field of a monochromatic electromagnetic wave with frequency $\omega$ and electric field amplitude $E_0$, which propagates in vacuum along the z-axis, and is polarized along the x-axis, (Fig. 2.1), i.e. $\frac{\vec{k}}{|k|} = \vec{e}_z$, and $\vec{e}(\vec{k}) = \vec{e}_x$. Then we obtain from Eqs.(2.18) and (2.19)

$$\vec{E}(\vec{r}, t) = E_0 \cos(\omega t - kz)\ \vec{e}_x, \tag{2.32}$$

and similiar for the magnetic field

$$\vec{H}(\vec{r}, t) = \frac{E_0}{Z_{F_0}} \cos(\omega t - kz)\ \vec{e}_y, \tag{2.33}$$

see Figure 2.1.

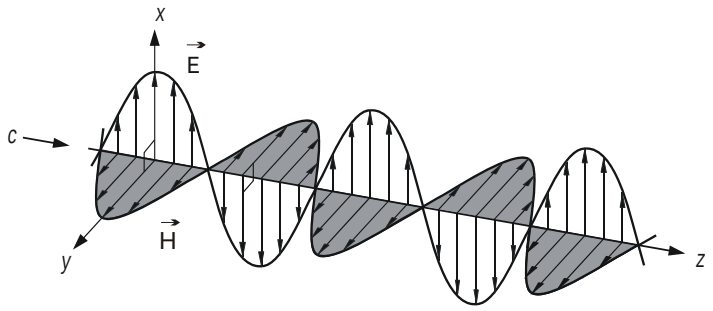


Figure 2.1: Transverse electromagnetic wave (TEM) [6]

Note, that for a backward propagating wave with $\vec{\underline{E}}(\vec{r}, t) = \underline{E}\ e^{\mathrm{j}\omega t + \mathrm{j}\vec{k}\cdot\vec{r}}\ \vec{e}_x$, and $\vec{\underline{H}}(\vec{r}, t) = \underline{H}\ e^{\mathrm{j}(\omega t + \vec{k}\vec{r})}\ \vec{e}_y$, there is a sign change for the magnetic field

$$\underline{H} = -\frac{|k|}{\mu_0 \omega} \underline{E}, \tag{2.34}$$

so that the $(\vec{k}, \vec{E}, \vec{H})$ always form a right handed orthogonal system.

### 2.1.3 Poynting Vectors, Energy Density and Intensity

The table below summarizes the instantaneous and time averaged energy content and energy transport related to an electromagnetic field

| Quantity | Real fields | Complex fields |
|---|---|---|
| Electric and magnetic energy density | $w_e = \frac{1}{2}\vec{E}\cdot\vec{D} = \frac{1}{2}\epsilon_0\epsilon_r\vec{E}^2$<br>$w_m = \frac{1}{2}\vec{H}\cdot\vec{B} = \frac{1}{2}\mu_0\mu_r\vec{H}^2$<br>$w = w_e + w_m$ | $\langle w_e\rangle = \frac{1}{4}\epsilon_0\epsilon_r\left\lvert\underline{\vec{E}}\right\rvert^2$<br>$\langle w_m\rangle = \frac{1}{4}\mu_0\mu_r\left\lvert\underline{\vec{H}}\right\rvert^2$<br>$\langle w\rangle = \langle w_e\rangle + \langle w_m\rangle$ |
| Poynting vector | $\vec{S} = \vec{E}\times\vec{H}$ | $\underline{\vec{T}} = \frac{1}{2}\underline{\vec{E}}\times\underline{\vec{H}}^*$ |
| Poynting theorem | $\mathrm{div}\vec{S} + \vec{E}\cdot\vec{j} + \frac{\partial w}{\partial t} = 0$ | $\mathrm{div}\vec{T} + \frac{1}{2}\underline{\vec{E}}\cdot\underline{\vec{j}}^* +$<br>$+2j\omega(\langle w_m\rangle - \langle w_e\rangle) = 0$ |
| Intensity | $I = \left\lvert\vec{S}\right\rvert = cw$ | $I = \mathrm{Re}\{\underline{\vec{T}}\} = c\langle w\rangle$ |

Table 2.1: Poynting vector and energy density in EM-fields

For a plane wave with an electric field $\underline{\vec{E}}(\vec{r},t) = \underline{E}e^{\mathrm{j}(\omega t - kz)}\ \vec{e}_x$ in a lossless medium, i.e. $\epsilon_r$ = real,we obtain for the time averaged energy density in units of [J/m$^3$]

$$\langle w\rangle = \frac{1}{2}\epsilon_r\epsilon_0|\underline{E}|^2, \tag{2.35}$$

the complex Poynting vector

$$\underline{\vec{T}} = \frac{1}{2Z_F}|\underline{E}|^2\ \vec{e}_z, \tag{2.36}$$

and the intensity in units of [W/m$^2$]

$$I = \frac{1}{2Z_F}|\underline{E}|^2 = \frac{1}{2}Z_F|\underline{H}|^2. \tag{2.37}$$

## 2.2 Paraxial Wave Equation

We start from the Helmholtz Equation (2.17)

$$\left(\Delta + k_0^2\right)\widetilde{\vec{E}}(x,y,z,\omega) = 0, \tag{2.38}$$

with the free space wavenumber $k_0 = \omega/c_0$. This equation can easily be solved in the Fourier domain, and one set of solutions are of course the plane waves with wave vector $|\vec{k}|^2 = k_0^2$. We look for solutions which are polarized in $x$-direction

$$\widetilde{\vec{E}}(x,y,z,\omega) = \widetilde{E}(x,y,z)\ \vec{e}_x. \tag{2.39}$$

We want to construct a beam with finite transverse extent into the x-y-plane and which is mainly propagating into the positive $z$-direction. As such we may try a superposition of plane waves with a dominant $z$-component of the k-vector, see Figure 2.2. The $k$-vectors can be written as

$$\begin{aligned} k_z &= \sqrt{k_0^2 - k_x^2 - k_y^2}, \\ &\approx k_0 \left(1 - \frac{k_x^2 + k_y^2}{2k_0^2}\right). \end{aligned} \tag{2.40}$$

with $k_x, k_y << k_0$.

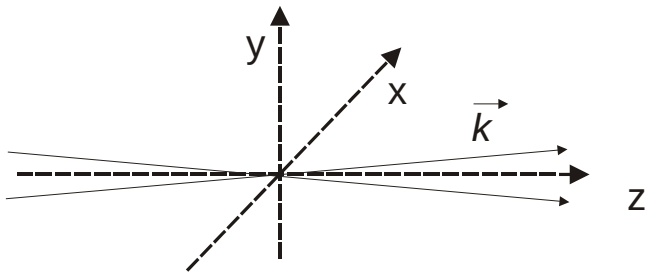


Figure 2.2: Construction of a paraxial beam by superimposing many plane waves with a dominante k-component in z-direction.

Then we obtain for the propagating field

$$\begin{aligned} \widetilde{E}(x,y,z) &= \int_{-\infty}^{+\infty}\int_{-\infty}^{+\infty} \widetilde{E}_0(k_x,k_y)\cdot \\ &\quad \exp\left[-jk_0\left(1-\frac{k_x^2+k_y^2}{2k_0^2}\right)z - jk_x x - jk_y y\right] dk_x dk_y, \\ &= \int_{-\infty}^{+\infty}\int_{-\infty}^{+\infty} \widetilde{E}_0(k_x,k_y)\cdot \\ &\quad \exp\left[j\left(\frac{k_x^2+k_y^2}{2k_0}\right)z - jk_x x - jk_y y\right] dk_x dk_y e^{-jk_0 z}, \end{aligned} \tag{2.41}$$

where $\widetilde{E}_0(k_x, k_y)$ is the amplitude for the waves with the corresponding transverse $k$-component. This function should only be nonzero within a small

range $k_x, k_y \ll k_0$. The function

$$\widetilde{E}_0(x,y,z) = \int_{-\infty}^{+\infty}\int_{-\infty}^{+\infty} \widetilde{E}_0(k_x,k_y)\exp\left[j\left(\frac{k_x^2+k_y^2}{2k_0}\right)z - jk_x x - jk_y y\right]dk_x dk_y \tag{2.42}$$

is a slowly varying function in the transverse directions $x$ and $y$, and it can be easily verified that it fulfills the paraxial wave equation

$$\frac{\partial}{\partial z}\widetilde{E}_0(x,y,z) = \frac{-j}{2k_0}\left(\frac{\partial^2}{\partial x^2}+\frac{\partial^2}{\partial x^2}\right)\widetilde{E}_0(x,y,z). \tag{2.43}$$

Note, that this equation is in its structure identical to the dispersive spreading of an optical pulse. The difference is that this spreading occurs now in the two transverse dimensions and is called diffraction.

## 2.3 Gaussian Beams

Since the kernel in Eq.(2.42) is quadratic in the transverse $k$-components using a two-dimensional Gaussian for the amplitude distribution leads to a beam in real space which is also Gaussian in the radial direction because of the resulting Gaussian integral. By choosing for the transverse amplitude distribution

$$\widetilde{E}_0(k_x,k_y) \sim \exp\left[-\frac{k_x^2+k_y^2}{2k_T^2}\right], \tag{2.44}$$

Eq.(2.42) can be rewritten as

$$\widetilde{E}_0(x,y,z) \sim \int_{-\infty}^{+\infty}\int_{-\infty}^{+\infty} \exp\left[j\left(\frac{k_x^2+k_y^2}{2k_0}\right)(z+jz_R) - jk_x x - jk_y y\right]dk_x dk_y, \tag{2.45}$$

with the parameter $z_R = k_0/k_T^2$, which we will later identify as the Rayleigh range. Thus, Gaussian beam solutions with different finite transverse width in $k$-space and real space behave as if they propagate along the z-axis with different imaginary z-component $z_R$. Carrying out the Fourier transformation results in the Gaussian Beam in real space

$$\widetilde{E}_0(x,y,z) \sim \frac{j}{z+jz_R}\exp\left[-jk_0\left(\frac{x^2+y^2}{2(z+jz_R)}\right)\right]. \tag{2.46}$$

The Gaussian beam is often formulated in terms of the complex beam parameter or $q$-parameter.

The propagation of the beam in free space and later even through optical imaging systems can be efficiently described by a proper transformation of the $q$-parameter

$$\widetilde{E}_0(r,z) \sim \frac{1}{q(z)} \exp\left[-jk_0\left(\frac{r^2}{2q(z)}\right)\right]. \tag{2.47}$$

Free space propagation is then described by

$$q(z) = z + jz_R \tag{2.48}$$

Using the inverse $q$-parameter, decomposed in real and imagniary parts,

$$\frac{1}{q(z)} = \frac{1}{R(z)} - j\frac{\lambda}{\pi w^2(z)}. \tag{2.49}$$

leads to

$$\widetilde{E}_0(r,z) = \frac{\sqrt{4Z_{F_0}P}}{\sqrt{\pi}w(z)} \exp\left[-\frac{r^2}{w^2(z)} - jk_0\frac{r^2}{2R(z)} + j\zeta(z)\right]. \tag{2.50}$$

Thus $w(z)$ is the waist of the beam and $R(z)$ is the radius of the phase fronts. We normalized the beam such that the Gaussian beam intensity $I(z,r) = \left|\widetilde{E}_0(r,z)\right|^2/(2Z_{F_0})$ expressed in terms of the power $P$ carried by the beam is given by

$$I(r,z) = \frac{2P}{\pi w^2(z)} \exp\left[-\frac{2r^2}{w^2(z)}\right], \tag{2.51}$$

$$\text{i.e.} \quad P = \int_0^{\infty}\int_0^{2\pi} I(r,z)\; r dr\; d\varphi. \tag{2.52}$$

The use of the q-parameter simplifies the description of Gaussian beam propagation. In free space propagation from $z_1$ to $z_2$, the variation of the beam parameter $q$ is simply governed by

$$q_2 = q_1 + z_2 - z_1. \tag{2.53}$$

where $q_2$ and $q_1$ are the beam parameters at $z_1$ and $z_2$.

If the beam waist, at which the beam has a minimum spot size $w_0$ and a planar wavefront ($R = \infty$), is located at $z = 0$, the variations of the

beam spot size and the radius of curvature of the phase fronts are explicitly expressed as

$$w(z) = w_o \left[1 + \left(\frac{z}{z_R}\right)^2\right]^{1/2}, \tag{2.54}$$

and

$$R(z) = z \left[1 + \left(\frac{z_R}{z}\right)^2\right], \tag{2.55}$$

where $z_R$ is called the Rayleigh range. The Rayleigh range is the distance over which the cross section of the beam doubles. The Rayleigh range is determined by the beam waist and the wavelength of light according to

$$z_R = \frac{\pi w_o^2}{\lambda}. \tag{2.56}$$

**Intensity**

Figure 2.3 shows the intensity of the Gaussian beam according to Eq.(2.51) for different propagation distances.

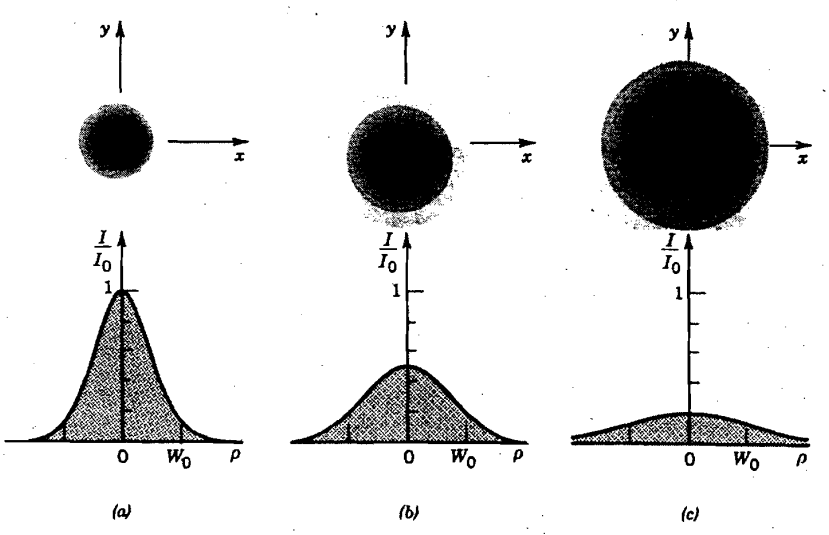


Figure 2.3: The normalized beam intensity $I/I_0$ as a function of the radial distance r at different axial distances: (a) z=0, (b) z=$z_R$, (c) z=2$z_R$.

The beam intensity can be rewritten as

$$I(r,z) = I_0 \frac{w_0^2}{w^2(z)} \exp\left[-\frac{2r^2}{w^2(z)}\right], \text{ with } I_0 = \frac{2P}{\pi w_0^2}. \tag{2.57}$$

For $z > z_R$ the beam radius growth linearly and therefore the area expands quadratically, which brings down the peak intensity quadratically with propagation distance.

On the beam axis ($r = 0$) the intensity is given by

$$I(r,z) = I_0 \frac{w_0^2}{w^2(z)} = \frac{I_0}{1 + \left(\frac{z}{z_R}\right)^2}. \tag{2.58}$$

The normalized beam intensity as a function of propagation distance is shown in Figure 2.4

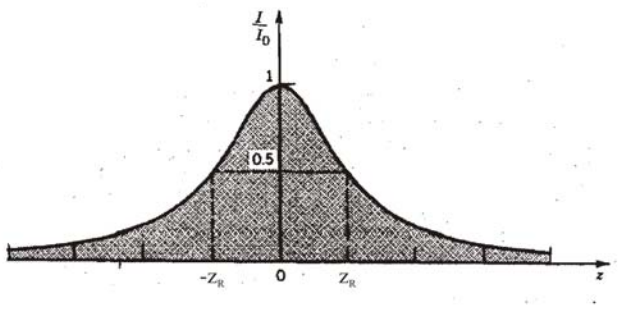


Figure 2.4: The normalized Beam intensity $I(r = 0)/I_0$ on the beam axis as a function of propagation distance $z$ [6], p. 84.

### Power

The fraction of the total power contained in the beam up to a certain radius is

$$\begin{aligned} \frac{P(r < r_0)}{P} &= \frac{2\pi}{P} \int_0^{r_0} I(r,z) r dr \\ &= \frac{4}{w^2(z)} \int_0^{r_0} \exp\left[-\frac{2r^2}{w^2(z)}\right] r dr \\ &= 1 - \exp\left[-\frac{2r_0^2}{w^2(z)}\right]. \end{aligned} \tag{2.59}$$

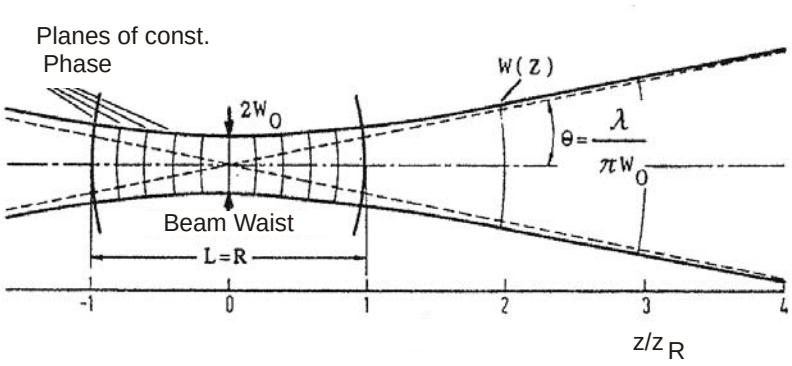


Figure 2.5: Gaussian beam and its characteristics.

Thus, there is a certain fraction of power within a certain radius of the beam

$$\frac{P(r < w(z))}{P} = 0.86, \tag{2.60}$$

$$\frac{P(r < 1.5w(z))}{P} = 0.99. \tag{2.61}$$

### Beam radius

Due to diffraction, the smaller the spot size at the beam waist, the faster the beam diverges according to 2.54 as illustrated in Figure **??**.

### Beam divergence

The angular divergence of the beam is inversely proportional to the beam waist. In the far field, the half angle divergence is given by

$$\theta = \frac{\lambda}{\pi w_o}, \tag{2.62}$$

see Figure 2.5.

### Confocal parameter and depth of focus

In linear microscopy, only a layer which has the thickness over which the beam is focused, called depth of focus, will contribute to a sharp image. In nonlinear microscopy (see problem set) only a volume on the order of beam cross section times depth of focus contributes to the signal. Therefore, the depth of focus or confocal parameter of the Gaussian beam, is the distance over which the beam stays focused and is defined as twice the Rayleigh range

$$b = 2z_R = \frac{2\pi w_o^2}{\lambda}. \tag{2.63}$$

The confocal parameter depends linear on the spot size (area) of the beam and is inverse to the wavelength of light. At a wavelength of $1\mu m$ a beam with a radius of $w_o = 1cm$,.the beam will stay focussed ove distances as long 600m. However, if the beam is stronlgy focussed down to $w_o = 10\mu m$ the field of depth is only $600\mu$m.

### Phase

The phase delay of the Gaussian beam is

$$\Phi(r,z) = k_0 z - \zeta(z) + k_0 \frac{r^2}{2R(z)} \tag{2.64}$$

$$\zeta(z) = \arctan\left(\frac{z}{z_R}\right). \tag{2.65}$$

On beam axis, there is the additional phase $\zeta(z)$ when the beam undergoes focussing as shown in Figure 2.6. This is in addition to the phase shift that a uniform plane wave already aquires.

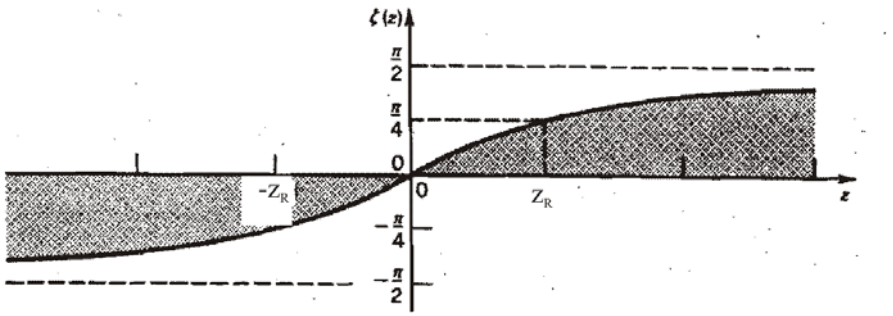


Figure 2.6: Phase delay of a Gaussian beam relative to a uniform plane wave on the beam axis [6], p. 87. This phase shift is known as Guoy-Phase-Shift.

This effect is known as Guoy-Phase-Shift. The third term in the phase shift is parabolic in the radius and describes the wavefront (planes of constant phase) bending due to the focusing, i.e. distortion from the uniform plane wave.

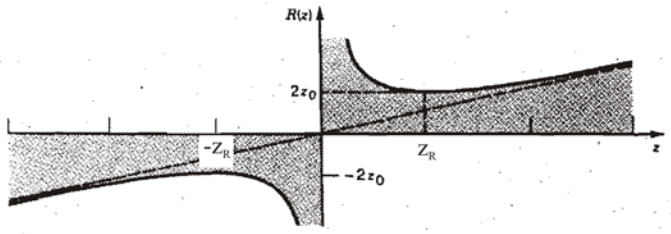


Figure 2.7: The radius of curvature $R(z)$ of the wavefronts of a Gaussian beam [6], p. 89.

The surfaces of constant phase are determined by $k_0 z - \zeta(z) + k_0 \frac{r^2}{2R(z)} = const.$ Since the radius of curvature $R(z)$ and the additional phase $\zeta(z)$ are slowly varying functions of $z$, i.e. they are constant over the radial variation of the wavefront, the wavefronts are paraboloidal surfaces with radius $R(z)$, see Figures 2.7 and 2.8.

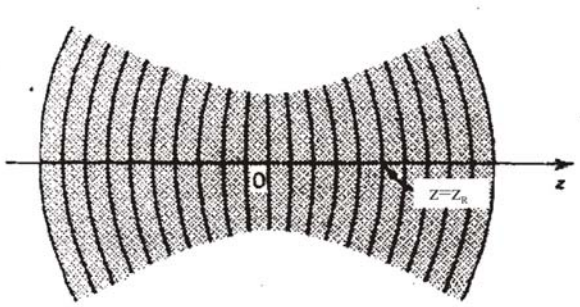


Figure 2.8: Wavefronts of a Gaussian beam, [6] p. 88.

For comparison, Figure 2.9 shows the wavefront of (a) a uniform plane wave, (b) a spherical wave and (c) a Gaussian beam. At points near the beam center, the Gaussian beam resembles a plane wave. At large z, the beam behaves like a spherical wave except that the phase fronts are delayed by a quarter of the wavlength due to the Guoy-Phase-Shift.

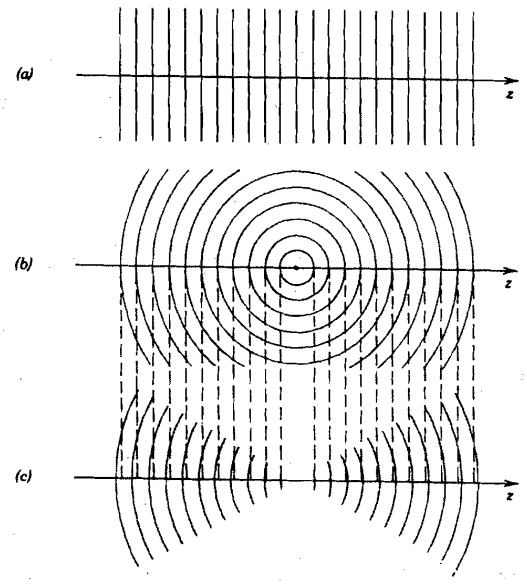


Figure 2.9: Wavefronts of (a) a uniform plane wave;(b) a spherical wave; (c) a Gaussian beam [5], p. 89.

## 2.4 Ray Propagation

A ray propagating in an optical system, see Figure 2.10, can be described by its position $r$ with respect to the optical axis and its inclination with respect to the optical axis $r'$. It is advantageous to use not $(r, r')$ as the ray coordinates but the combination $(r, n\ r')$, where $n$ is the local refractive index at the position of the ray. Due to propagation, the ray coordinates may change, which can be desribed by a marix, that maps initial position and inclination into the corresponding quantitaties after the propagation

$$\begin{pmatrix} r_2 \\ n_2 r_2' \end{pmatrix} = \begin{pmatrix} A & B \\ C & D \end{pmatrix} \begin{pmatrix} r_1 \\ n_1 r_1' \end{pmatrix}. \tag{2.66}$$

This imaging matrix is called an ABCD-matrix.

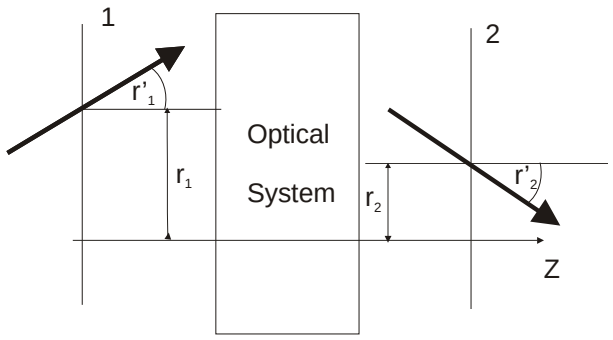


Figure 2.10: Description of optical ray propagation by its distance and inclination from the optical axis

The advantage in using $(r, n\ r')$ as the ray coordinates is that it preserves the phase space volume, i.e. for lossless optical systems the determinant of the ABCD-matrix must be 1. Also Snell's law for paraxial rays has then a simple form, see Figure 2.11. For paraxial rays the angles to the interface normal, $\theta_1$ and $\theta_2$, are much smaller than 1, and we can write

$$r_1' = \tan\theta_1 \approx \sin\theta_1 \approx \theta_1, \text{ and } r_2' = \tan\theta_2 \approx \sin\theta_2 \approx \theta_2.$$

Then Snell's law is

$$n_1\ r_1' = n_2\ r_2'. \tag{2.67}$$

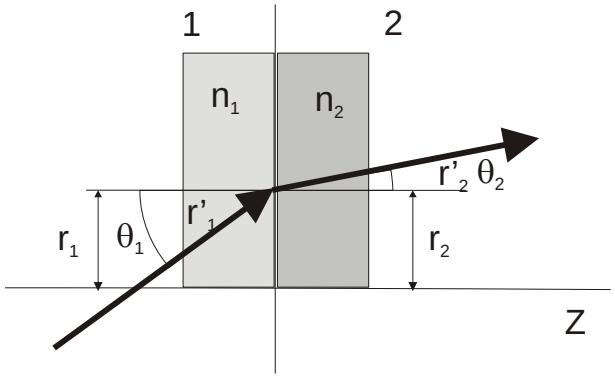


Figure 2.11: Snell's law for paraxial rays

The ABCD-matrix describing a ray going from a medium with index $n_1$ to a medium with index $n_2$ is the unity matrix

$$\begin{aligned} r_2 &= r_1 && (2.68)\\ n_2\, r_2' &= n_1\, r_1'. && (2.69) \end{aligned}$$

**Free space propagation**

For propagation in free space, see Figure 2.12, the relationship between input and output ray parameters is

$$\begin{aligned} r_2 &= r_1 + r_1' \cdot L \\ r_2' &= r_1' \end{aligned}$$

or the propagation matrix is

$$\mathbf{M} = \begin{pmatrix} 1 & L \\ 0 & 1 \end{pmatrix}. \qquad (2.70)$$

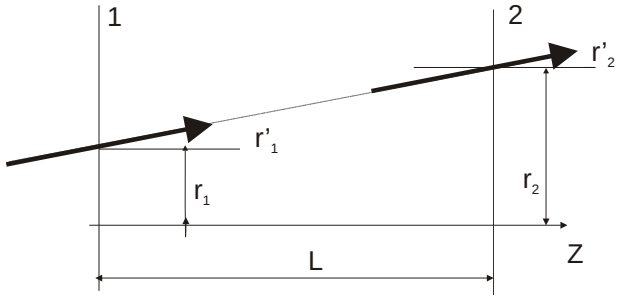


Figure 2.12: Free space propagation

### Propagation in medium with length L and index $n$

Free propagation through a medium with index $n$ does result in a reduced position shift with respect to the optical axis in comparison to free space, because the beam is first bent to the optical axis according to Snell's law, see Figure 2.13. Therefore the corresponding ABCD-matrix is

$$\mathbf{M} = \begin{pmatrix} 1 & L/n \\ 0 & 1 \end{pmatrix}. \tag{2.71}$$

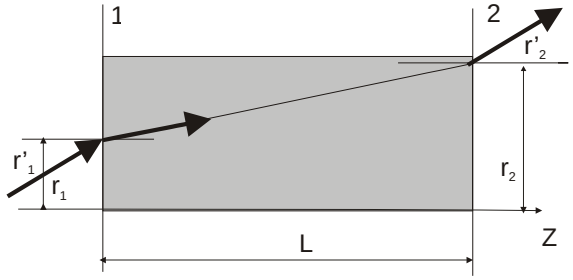


Figure 2.13: Ray propagation through a medium with refractive index $n$, shortens the path length of the beam by a factor of $n$.

### Parbolic surface or thin lens

**Plano-Convex Lens** When a ray penetrates a parabolic surface between two media with refractive indices $n_1$ and $n_2$, it changes its inclination. A

parabolic surface can be closely approximated by the surface of a sphere, see Figure 2.14. Snells law in paraxial approximation is

$$n_1 \ (r_1' + \alpha) = n_2 \ (r_2' + \alpha) \, . \tag{2.72}$$

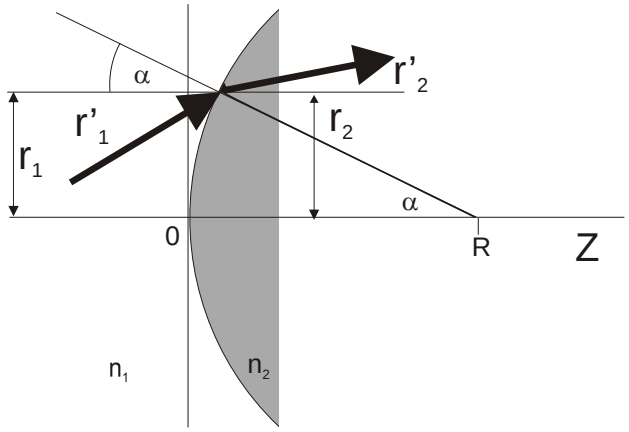


Figure 2.14: Derivation of ABCD-matrix of a thin plano-convex lens.

The small angle $\alpha$ can be approximated by $\alpha \approx r_1/R$. In total we then obtain the mapping

$$r_2 = r_1 \tag{2.73}$$

$$n_2 \ r_2' = n_1 \ r_1' + \frac{n_1 - n_2}{R} r_1 \tag{2.74}$$

or

$$\mathbf{M} = \begin{pmatrix} 1 & 0 \\ \frac{n_1 - n_2}{R} & 1 \end{pmatrix} . \tag{2.75}$$

Note, the second normal interface does not change the ray propagation matrix and therefore Eq.(2.75) describes correctly the ray propagation through a thin plano-convex lens.

**Biconvex Lens** If the lens would have a second convex surface, this would refract the ray twice as strongly and we would obtain

$$\mathbf{M} = \begin{pmatrix} 1 & 0 \\ 2\frac{n_1 - n_2}{R} & 1 \end{pmatrix} . \tag{2.76}$$

The quantity $2\frac{n_2-n_1}{R}$ is called the refractive strength of the biconvex lense or inverse focal length $1/f$.Because the system of a thin lens plus free space propagation results in the matrix (calculated in the reverse order)

$$\mathbf{M}_{tot} = \begin{pmatrix} 1 & f \\ 0 & 1 \end{pmatrix} \begin{pmatrix} 1 & 0 \\ -\frac{1}{f} & 1 \end{pmatrix} = \begin{pmatrix} 0 & f \\ -\frac{1}{f} & 1 \end{pmatrix}, \tag{2.77}$$

which ensures that each ray parallel to the optical axis goes through the on axis focal point at the end of the free space section, see Figure 2.15.

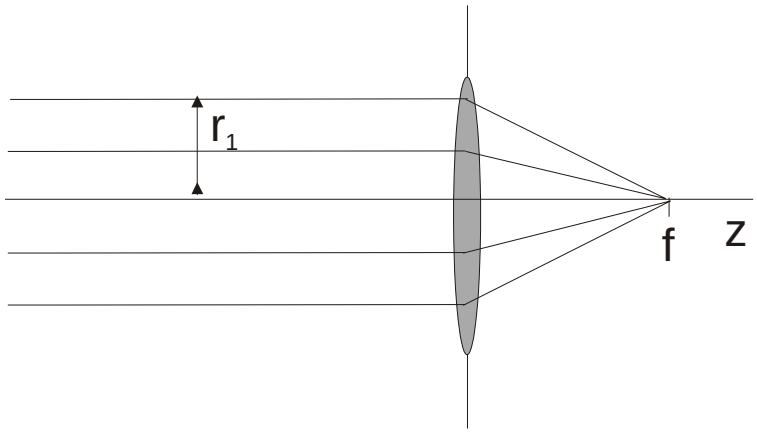


Figure 2.15: Imaging of parallel rays through a lens with focal length $f$.

### Curved Mirrors

Other often used optical components in imaging systems are curved mirrors with radius of curvature $ROC = R$, see Figure 2.16. The advantage of reflective optics is that the rays don't have to pass through dispersive material like through a lense, which is very disturbing for ultrashort pulses.

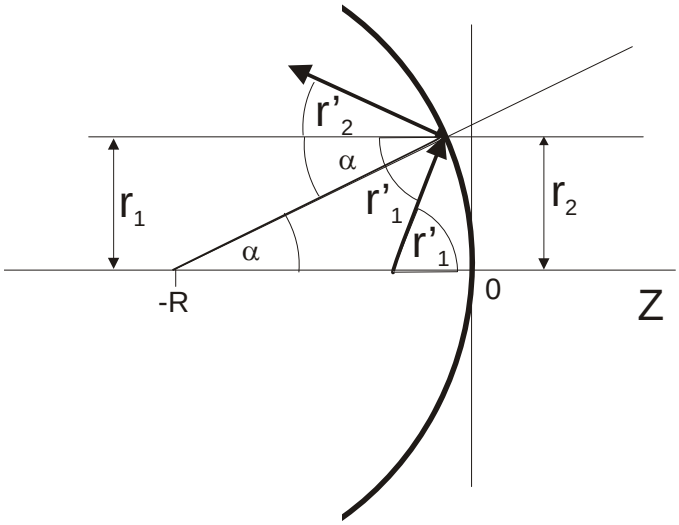


Figure 2.16: Derivation of ray matrix for concave mirror with Radius R.

As in the case of the thin lens,e the imaging does not change the distance of the ray from the optical axis, however, the slope of the rays obey

$$r_1' - \alpha = r_2' + \alpha. \tag{2.78}$$

with $\alpha \approx r_1/R$ in paraxial approximation. Therefore the ABCD matrix describing the reflection of rays at a curved mirror with $ROC = R$ is

$$\mathbf{M} = \begin{pmatrix} 1 & 0 \\ -\frac{1}{f} & 1 \end{pmatrix}, \text{ with } f = \frac{R}{2}. \tag{2.79}$$

Gauss' Lens Formula:

As a simple application of the ray matrices for optical system design, we derive Gauss' lens formula, which says that all rays emitted from an orignial placed a distance $d_1$ from a lens with focal length $f$ form an image at a distance $d_2$, which is related to $d_1$ by

$$\frac{1}{d_1} + \frac{1}{d_2} = \frac{1}{f}, \tag{2.80}$$

see Figure 2.17.

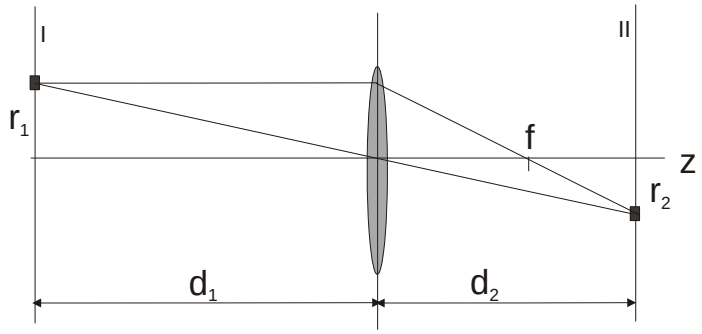


Figure 2.17: Gauss' lens formula.

The magnification of the lens system is $M_r = \frac{r_2}{r_1} = \frac{d_2}{d_1} = \left|\frac{f}{d_1 - f}\right|$. The ray matrix that describes the imagaing from the orignal plane I to the image plane II is described by the product

$$\begin{aligned}\begin{pmatrix} A & B \\ C & D \end{pmatrix} &= \begin{pmatrix} 1 & d_2 \\ 0 & 1 \end{pmatrix}\begin{pmatrix} 1 & 0 \\ -\frac{1}{f} & 1 \end{pmatrix}\begin{pmatrix} 1 & d_1 \\ 0 & 1 \end{pmatrix} \\ &= \begin{pmatrix} 1 - \frac{d_2}{f} & \left(1 - \frac{d_2}{f}\right) d_1 + d_2 \\ -\frac{1}{f} & 1 - \frac{d_1}{f} \end{pmatrix}. \end{aligned} \tag{2.81}$$

In order that the distance $r_2$ only depends on $r_1$, but not on $r_1'$, $B$ must be 0, which is Eq. (2.80). Thus in total we have

| | |
|---|---|
| Magnification | $M_r = \left\lvert\frac{f}{d_1 - f}\right\rvert$ |
| Distance to focus | $d_2 - f = M_r^2 (d_1 - f)$ |

(2.82)

More complicated imaging systems, such as thick lenses, can be described by ray matrices and arbitrary paraxial optical systems can be analyzed with them, which shall not be pursued further here. Rather, we want to study how Gaussian beams are imaged by paraxial optical systems

## 2.5 Gaussian Beam Propagation

The propagation of Gaussian beams through paraxial optical systems can be efficiently evaluated using the ABCD-law [4], which states that the q-parameter of a Gaussian beam passing a optical system described by an

ABCD-marix is given by

$$q_2 = \frac{Aq_1 + B}{Cq_1 + D}, \tag{2.83}$$

where $q_1$ and $q_2$ are the beam parameters at the input and the output planes of the optical system or component, see Figure 2.18

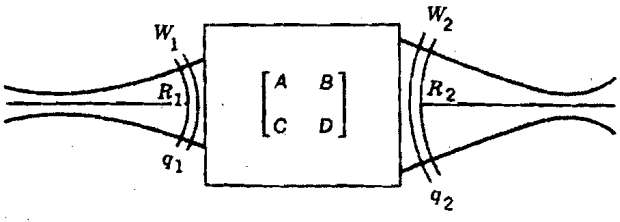


Figure 2.18: Gaussian beam transformation by ABCD law, [6], p. 99.

To proove this law, we realize that it is true for the case of free space propagation, i.e. pure diffraction, comparing (2.83) with (2.53) and (2.70). If we can proove that it is additionally true for a thin lens, then we are finished, because every ABCD matrix (2x2 matrix) can be written as a product of a lower and upper triangular matrix (LR-decomposition) like the one for free space propagation and the thin lens. Note, the action of the lens is identical to the action of free space propagation, but in the Fourier-domain. In the Fourier domain the Gaussian beam parameter is replaced by its inverse (2.46)

$$\widetilde{E}_0(x, y, z) = \frac{j}{q(z)} \exp\left[-jk_0\left(\frac{x^2 + y^2}{2q(z)}\right)\right]. \tag{2.84}$$

$$\widetilde{E}_0(k_z, k_y, z) = 2\pi j \exp\left[-jq(z)\left(\frac{k_z^2 + k_y^2}{2k_0}\right)\right] \tag{2.85}$$

But the inverse q-parameter transforms according to (2.83)

$$\frac{1}{q_2} = \frac{D\frac{1}{q_1} + C}{B\frac{1}{q_1} + A}, \tag{2.86}$$

which leads for a thin lens to

$$\frac{1}{q_2} = \frac{1}{q_1} - \frac{1}{f}. \tag{2.87}$$

This is exactly what a thin lens does, see Eq.(2.49), it changes the radius of curvature of the phase front but not the waist of the beam according to

$$\frac{1}{R_2} = \frac{1}{R_1} - \frac{1}{f}. \tag{2.88}$$

With that finding, we have proven the ABCD law for Gaussian beam propagation through paraxial optical systems.

The ABCD-matrices of the optical elements discussed so far including nonnomal incidence are summarized in Table 2.2. As an application of the

| Optical Element | ABCD-Matrix |
|---|---|
| Propagation in Medium with index $n$ and length $L$ | $\begin{pmatrix} 1 & L/n \\ 0 & 1 \end{pmatrix}$ |
| Thin Lens with focal length $f$ | $\begin{pmatrix} 1 & 0 \\ -1/f & 1 \end{pmatrix}$ |
| Mirror under Angle $\theta$ to Axis and Radius $R$ Sagittal Plane | $\begin{pmatrix} 1 & 0 \\ \frac{-2\cos\theta}{R} & 1 \end{pmatrix}$ |
| Mirror under Angle $\theta$ to Axis and Radius $R$ Tangential Plane | $\begin{pmatrix} 1 & 0 \\ \frac{-2}{R\cos\theta} & 1 \end{pmatrix}$ |
| Brewster Plate under Angle $\theta$ to Axis and Thickness $d$, Sagittal Plane | $\begin{pmatrix} 1 & \frac{d}{n} \\ 0 & 1 \end{pmatrix}$ |
| Brewster Plate under Angle $\theta$ to Axis and Thickness $d$, Tangential Plane | $\begin{pmatrix} 1 & \frac{d}{n^3} \\ 0 & 1 \end{pmatrix}$ |

Table 2.2: ABCD matrices for commonly used optical elements.

Gaussian beam propagation, lets consider the imaging of a Gaussian beam with a waist $w_{01}$ by a thin lens at a distance $d_1$ away from the waist to a beam with a different size $w_{02}$, see Figure 2.19.

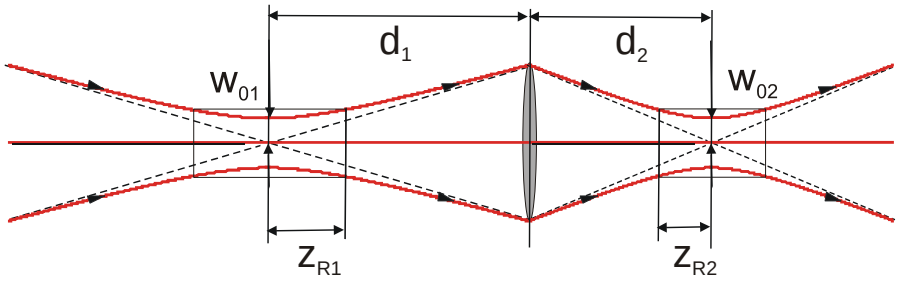


Figure 2.19: Focusing of a Gaussian beam by a lens.

There will be a new focus at a distance $d_2$.The corresponding ABCD matrix is of course the one from Eq.(2.81), which is repeated here

$$\begin{pmatrix} A & B \\ C & D \end{pmatrix} = \begin{pmatrix} 1-\frac{d_2}{f} & \left(1-\frac{d_2}{f}\right) d_1 + d_2 \\ -\frac{1}{f} & 1-\frac{d_1}{f} \end{pmatrix}. \tag{2.89}$$

The q-parameter of the Gaussian beam at the position of minimum waist is purely imaginary $q_1 = jz_{R1} = j\frac{\pi w_{01}^2}{\lambda}$ and $q_2 = jz_{R2} = j\frac{\pi w_{02}^2}{\lambda}$, where

$$q_2 = \frac{A\ q_1 + B}{C\ q_1 + D} = \frac{jz_{R1}A + B}{jz_{R1}C + D} = \frac{jz_{R1}A + B}{jz_{R1}C + D} = jz_{R2}. \tag{2.90}$$

In the limit of ray optics, where the beam waists can be considered to by zero, i.e. $z_{R1} = z_{R2} = 0$ we obtain $B = 0$, i.e. the imaging rule of classical ray optics Eq.(2.80). It should not come at a surprise that for the Gaussian beam propagation this law does not determine the exact distance $d_2$ of the position of the new waist. Because, in the ray analysis we neglected diffraction. Therefore, the Gaussian beam analysis, although it uses the same description of the optical components, gives a slightly different and improved answer for the position of the focal point. To find the position $d_2$, we request that the real part of the right hand side of (2.90) is zero,

$$BD - z_{R1}^2 AC = 0 \tag{2.91}$$

which can be rewritten as

$$\frac{1}{d_2} = \frac{1}{f} - \frac{1}{d_1 + \frac{z_{R1}^2}{d_1 - f}}. \tag{2.92}$$

Again for $z_{R1} \to 0$, we obtain the ray optics result. And the imaginary part of Eq.(2.90) leads to

$$\frac{1}{z_{R2}} = \frac{1}{z_{R1}} \left( D^2 + z_{R1}^2 C^2 \right), \tag{2.93}$$

or

$$\frac{1}{w_{02}^2} = \frac{1}{w_{01}^2} \left( 1 - \frac{d_1}{f} \right)^2 \left[ 1 + \left( \frac{z_{R1}}{d_1 - f} \right)^2 \right]. \tag{2.94}$$

With the magnification $M$ for the spot size, with is closely related to the Magnification $M_r$ of ray optics, we can rewrite the results as

| | |
|---|---|
| Magnification | $M = M_r/\sqrt{1+\xi^2}$, with $\xi = \frac{z_{R1}}{d_1 - f}$ and $M_r = \frac{f}{d_1 - f}$ |
| Beam waist | $w_{02} = M \cdot w_{01}$ |
| Confocal parameter | $2z_{R2} = M^2\ 2z_{R2}$ |
| Distance to focus | $d_2 - f = M^2 (d_1 - f)$ |
| Divergence | $\theta_{02} = \theta_{01}/M$ |

(2.95)

## 2.6 Optical Resonators

With the Gaussian beam solutions, we can finally construct optical resonators with finite transverse extent, i.e. real Fabry-Perots. To do that we insert into the Gaussian beam, see Figure 2.20, curved mirrors with the proper radius of curvature, such that the beam is imaged upon itself.

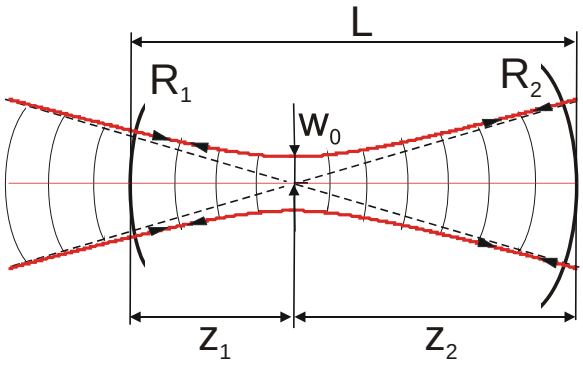


Figure 2.20: Fabry-Perot resonator with finite beam cross section by inserting curved mirrors into the beam to back reflect the beam onto itself.

### Curved-Flat Mirror Resonator

We first consider the simple resonator constructed by a curved and flat mirror, i.e. only the left side of the gaussian beam in Figure 2.20, see Figure 2.21

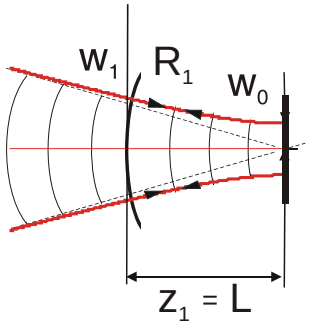


Figure 2.21: Curved-Flat Mirror Resonator

From Eqs.(2.54) and (2.55) we immediately get an expression for the radius of curvature of the mirror necessary to generate a certain confocal parameter $z_R = \frac{\pi w_o^2}{\lambda}$ or spot size on the flat mirror given a certain wavelength

$$w_1 = w_o \left[1 + \left(\frac{L}{z_R}\right)^2\right]^{1/2}, \tag{2.96}$$

and

$$R_1 = L\left[1 + \left(\frac{z_R}{L}\right)^2\right]. \tag{2.97}$$

Since the confocal parameter is a positive quantity it follows that we always need a mirror with a radius of curvature $R_1 > L$, to form a stable gaussian mode in the resonator. The spot size on the flat and curved mirrors in terms of the radius of curvature of the mirror and the distance of the mirror is

$$w_o = \sqrt{\frac{\lambda R_1}{\pi}} \sqrt[4]{\frac{L}{R_1}\left(1 - \frac{L}{R_1}\right)}, \tag{2.98}$$

and

$$w_1 = \sqrt{\frac{\lambda R_1}{\pi}} \sqrt[4]{\frac{\frac{L}{R_1}}{1 - \frac{L}{R_1}}}. \tag{2.99}$$

There is a resonator mode with finite size for $0 < L < R_1$, i.e. the cavity is stable in this parameter range.. Figure 2.22 shows the normalized beam radii on both mirrors as a function of the normalized distance between the mirrors $\frac{L}{R_1}$.

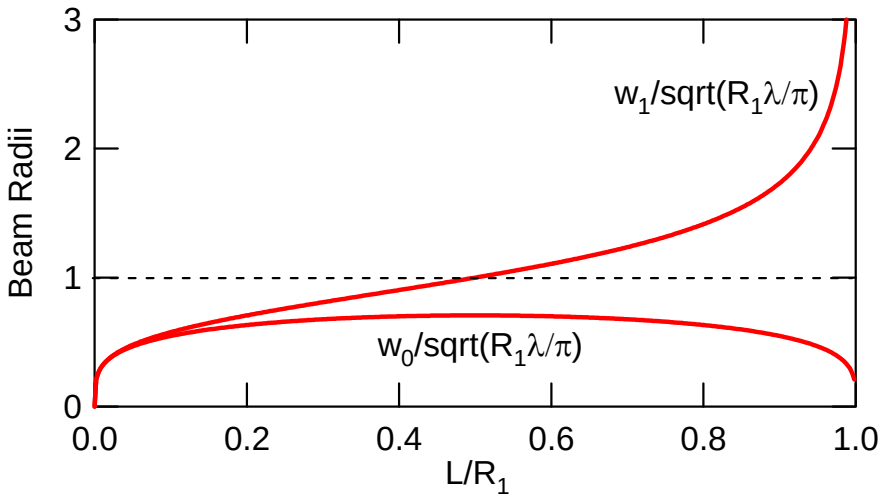


Figure 2.22: Beam waists of the curved-flat mirror resonator as a function of the cavity parameter $g_1$.

Note, that for a given curved mirror with radius of curvature $(ROC) = R_1$, the waist of the beam goes to zero for both extremes of the distance between the mirrors where the cavity is stable. There is a large central range around $L \approx R_1/2$, where the beam waist is maximum and insensitive to the exact distance between the mirrors.

### Two-Curved Mirror Resonator

Now, we can analyze what happens for the case of a resonator with two curved mirrors as shown in Figure 2.20. The gaussian beam formulas Eqs.(2.54) and (2.55) give us now the following conditions for beam waists

$$w_1 = w_o \left[ 1 + \left( \frac{z_1}{z_R} \right)^2 \right]^{1/2}, \tag{2.100}$$

$$w_2 = w_o \left[ 1 + \left( \frac{z_2}{z_R} \right)^2 \right]^{1/2}, \tag{2.101}$$

$$R_1 = z_1 \left[ 1 + \left( \frac{z_R}{z_1} \right)^2 \right], \tag{2.102}$$

$$R_2 = z_2 \left[ 1 + \left( \frac{z_R}{z_2} \right)^2 \right], \tag{2.103}$$

and

$$L = z_1 + z_2. \tag{2.104}$$

The last three equations determine the confocal parameter $z_R$ and the distances between location of waist and mirrors $z_1$ and $z_2$ in dependence on the radii of curvature $R_1$, $R_2$ and the distance between mirrors $L$. It is straight forward to eliminate the confocal parameter from Eqs.(2.102), (2.103) and to solve the remaining equation together with Eq.(2.104) for the distances $z_1$ and $z_2$. The result is

$$z_1 = \frac{L(R_2 - L)}{R_1 + R_2 - 2L}, \tag{2.105}$$

and by symmetry

$$z_2 = \frac{L(R_1 - L)}{R_1 + R_2 - 2L} = L - z_1. \tag{2.106}$$

Resubstitution into Eq.(2.102) leads to an expression for the Rayleigh range of the beam and its waist

$$z_R^2 = L \frac{(R_1 - L)(R_2 - L)(R_1 + R_2 - L)}{(R_1 + R_2 - 2L)^2}. \tag{2.107}$$

and therefore

$$w_o^4 = \left( \frac{\lambda L}{\pi} \right)^2 \frac{(R_1 - L)(R_2 - L)(R_1 + R_2 - L)}{L(R_1 + R_2 - 2L)^2} \tag{2.108}$$

$$= \left( \frac{\lambda \sqrt{R_1 R_2}}{\pi} \right)^2 \frac{L^2}{R_1 R_2} \frac{(1 - \frac{L}{R_1})(1 - \frac{L}{R_2})(\frac{L}{R_1} + \frac{L}{R_2} - \frac{L}{R_1}\frac{L}{R_2})}{(\frac{L}{R_1} + \frac{L}{R_2} - 2\frac{L}{R_1}\frac{L}{R_2})^2}. \tag{2.109}$$

For completeness the spot size on the mirrors is given by

$$w_1^4 = \left(\frac{\lambda R_1}{\pi}\right)^2 \frac{R_2 - L}{R_1 - L}\left(\frac{L}{R_1 + R_2 - L}\right) \quad (2.110)$$

$$= \left(\frac{\lambda\sqrt{R_1 R_2}}{\pi}\right)^2 \frac{1-\frac{L}{R_2}}{1-\frac{L}{R_1}} \frac{\frac{L}{R_1}\frac{L}{R_2}}{\frac{L}{R_1} + \frac{L}{R_2} - \frac{L}{R_1}\frac{L}{R_2}}. \quad (2.111)$$

By symmetry, we find the spot size on mirror 2 by switching index 1 and 2:

$$w_2^4 = \left(\frac{\lambda R_2}{\pi}\right)^2 \frac{R_1 - L}{R_2 - L}\left(\frac{L}{R_1 + R_2 - L}\right) \quad (2.112)$$

$$= \left(\frac{\lambda\sqrt{R_1 R_2}}{\pi}\right)^2 \frac{1-\frac{L}{R_1}}{1-\frac{L}{R_2}} \frac{\frac{L}{R_1}\frac{L}{R_2}}{\frac{L}{R_1} + \frac{L}{R_2} - \frac{L}{R_1}\frac{L}{R_2}}. \quad (2.113)$$

The mode characteristics $w_0$, $w_1$, $w_2$, $z_1$ and $z_2$for the two-mirror resonator are shown in Figure 2.23 for the case $R_1 = 10$cm and $R_2 = 11$cm as a function of the mirror distance $L$

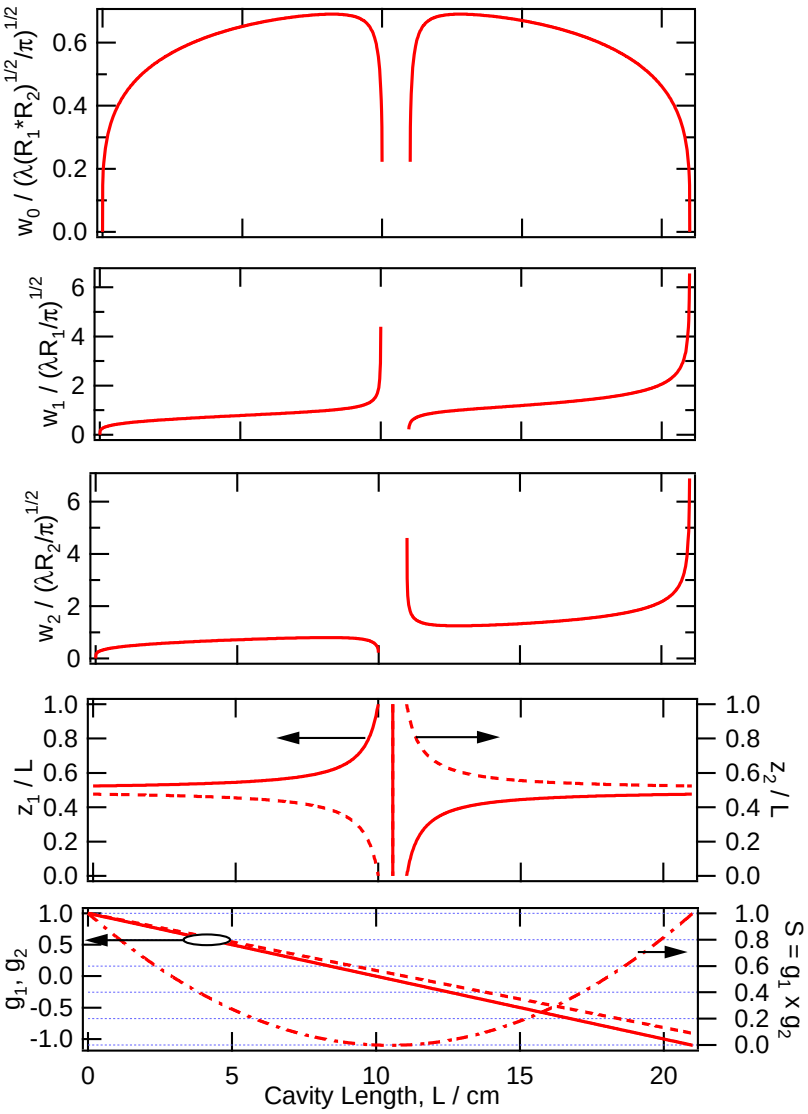


Figure 2.23: From top to bottom: two-mirror resonator mode characteristics $w_0$, $w_1$, $w_2$, $z_1$, $z_2$ and cavity parameters, $g_1$, $g_2$, $S$ for the case $R_1 = 10$ cm and $R_2 = 11$ cm.

**Resonator stability** As we can read of from Figure 2.23 for a two-mirror resonator with concave mirrors and $R_1 \leq R_2$, we obtain the general stability diagram as shown in Figure 2.24.

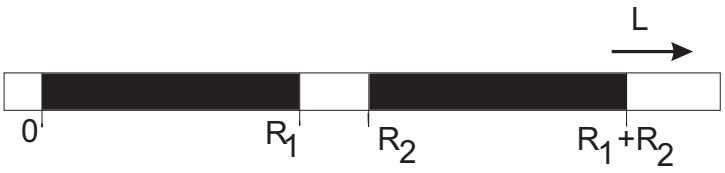


Figure 2.24: Stabile regions (black) for the two-mirror resonator.

There are two ranges for the mirror distance L, within which the cavity is stable, $0 \leq L \leq R_1$ and $R_2 \leq L \leq R_1 + R_2$.The stable and unstable parameter ranges can be expressed in a compact way in terms of the cavity parameters $g_1$ and $g_2$ defined by $g_i = (R_i - L)/R_i$, for $i = 1, 2$.These cavity parameters together and its product $S = g_1 \cdot g_2$ are shown in the last graph of Figure 2.23. The cavity mode has finite size, i.e. it is stable for

$$\text{stable} : 0 \leq g_1 \cdot g_2 = S \leq 1 \tag{2.114}$$

and unstable for

$$\text{unstable} : g_1 g_2 \leq 0; \text{ or } g_1 g_2 \geq 1. \tag{2.115}$$

The stability criterion can be easily interpreted geometrically. Of importance are the distances between the mirror mid-points $M_i$ and the cavity end points, i.e. $g_i = (R_i - L)/R_i = -S_i/R_i$, as shown in Figure 2.25.

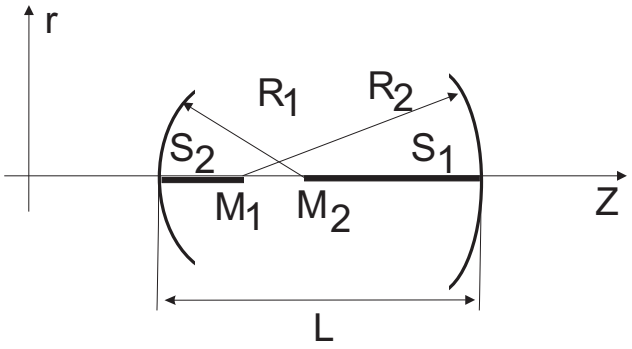


Figure 2.25: The stability criterion involves distances between the mirror mid-points $M_i$ and the cavity end points. i.e. $g_i = (R_i - L)/R_i = -S_i/R_i$.

The following rules for a stable resonator can be derived from Figure 2.25 using the stability criterion expressed in terms of the distances $S_i$. Note, that without proof, the distances and radii can be positive and negative, where the latter indicate concave mirrors

$$\text{stable} : 0 \leq \frac{S_1 S_2}{R_1 R_2} \leq 1. \tag{2.116}$$

This results in the following rules for the geometry of stable two-mirror resonators:

- A resonator is stable if the mirror radii, laid out along the optical axis, overlap.

- A resonator is unstable if the radii do not overlap or one lies within the other.

Figure 2.26 shows stable and unstable resonator configurations.

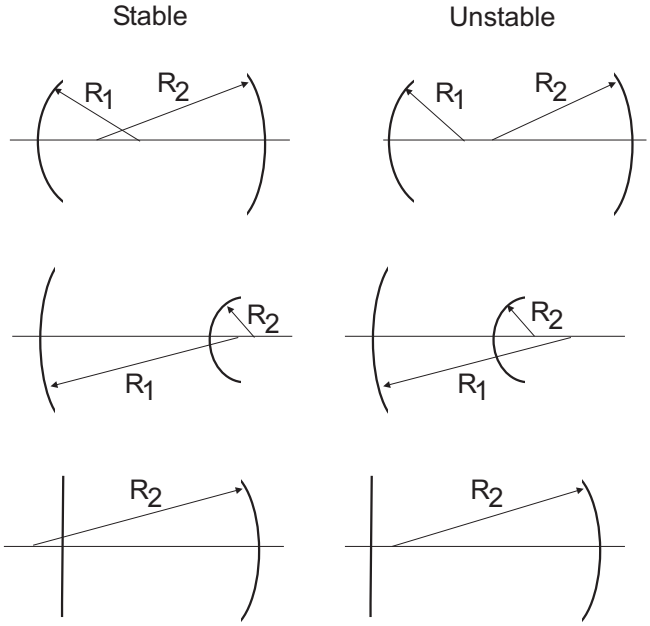


Figure 2.26: Illustration of stable and unstable resonator configurations.

### Hermite-Gaussian-Beams (TEM$_{mn}$-Beams)

It turns out that the Gaussian Beams are not the only solution to the paraxial wave equation (2.43). The stable modes of the resonator reproduce themselves after one round-trip,

$$\begin{aligned}\widetilde{E}_{m,n}(x,y,z) &= A_{m,n}\left[\frac{w_0}{w(z)}\right] G_m\left[\frac{\sqrt{2}x}{w(z)}\right] G_n\left[\frac{\sqrt{2}y}{w(z)}\right] \cdot \\ &\quad \exp\left[-jk_0\left(\frac{x^2+y^2}{2R(z)}\right) + j(m+n+1)\zeta(z)\right]\end{aligned} \tag{2.117}$$

where

$$G_m[u] = H_m[u]\exp\left[-\frac{u^2}{2}\right], \text{ for } m = 0,1,2,... \tag{2.118}$$

are the Hermite-Gaussians with the Hermite-Polynomials

$$\begin{aligned} H_0[u] &= 1, \\ H_1[u] &= 2u, \\ H_2[u] &= 4u^2 - 1, \\ H_3[u] &= 8u^3 - 12u, \end{aligned} \tag{2.119}$$

and $\zeta(z)$ is the Guoy-Phase-Shift according to Eq.(2.65). The lower order Hermite Gaussians are depicted in Figure 2.27

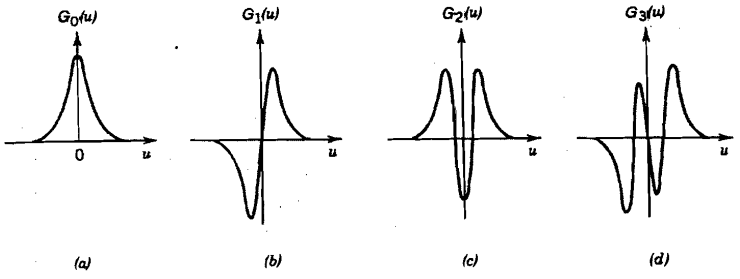


Figure 2.27: Hermite-Gauissians $G_m(u)$ for $m = 0, 1, 2$ and 3.

and the intensity profile of the first higher order resonator modes are shown in Figure 2.28.

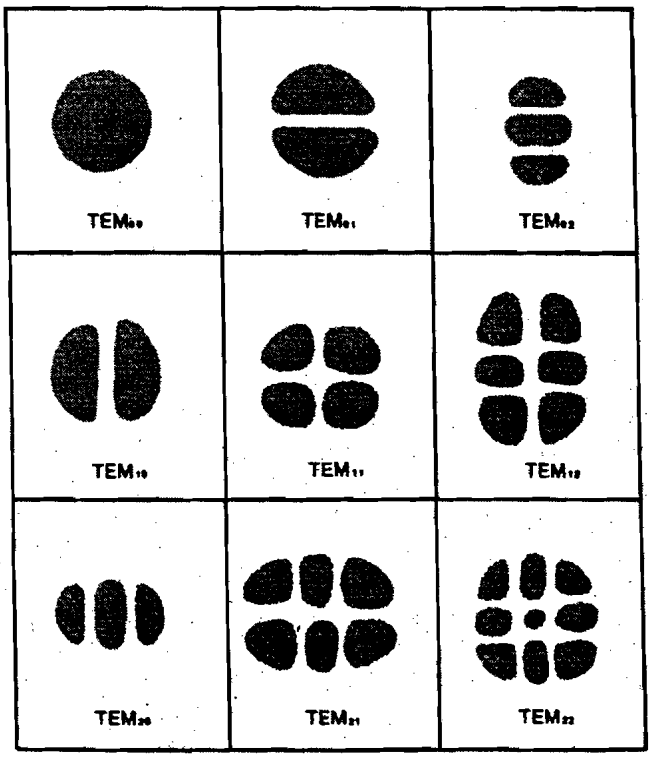


Figure 2.28: Intensity profile of $\mathrm{TEM}_{mn}$-beams, [6], p. 103.

Besides the different mode profiles, the higher order modes experience greater phase advances during propogation, because they are made up of $k$-vectors with larger transverse components.

### Axial Mode Structure

As we have seen for the Fabry-Perot resonator, the longitudinal modes are characterized by a roundtrip phase that is a multiple of $2\pi$. Back then, we did not consider transverse modes. Thus in a resonator with finite transverse beam size, we obtain an extended family of resonances, with distinguishable field patterns. The resonance frequencies $\omega_{pmn}$ are determined by the roundtrip phase condition

$$\phi_{plm} = 2p\pi, \text{ for } p = 0, \pm 1, \pm 2, ... \tag{2.120}$$

For the linear resonator according to Figure 2.20, the roundtrip phase of a Hermite-Gaussian $T_{plm}$-beam is

$$\phi_{plm} = 2kL - 2(l+m+1)\left(\zeta(z_2) - \zeta(z_1)\right), \tag{2.121}$$

where $\zeta(z_2) - \zeta(z_1)$ is the additional Guoy-Phase-Shift, when the beam goes through the focus once on its way from mirror 1 to mirror 2. Then the resonance circular frequencies are

$$\omega_{plm} = \frac{c}{L}\left[\pi p + (l+m+1)\left(\zeta(z_2) - \zeta(z_1)\right)\right] \tag{2.122}$$

If the Guoy-Phase-Shift is not a rational number times $\pi$, then all resonance frequencies are non degenerate. However, for the special case where the two mirrors have identical radius of curvature $R$ and are spaced a distance $L = R$ apart, which is called a confocal resonator, the Guoy-Phase-shift is $\zeta(z_2) - \zeta(z_1) = \pi/2$, with resonance frequencies

$$f_{plm} = \frac{c}{2L}\left[p + \frac{1}{2}(l+m+1)\right]. \tag{2.123}$$

In that case all even, i.e. $l+m$, transverse modes are degenerate to the longitudinal or fundamental modes, see Figure 2.29.

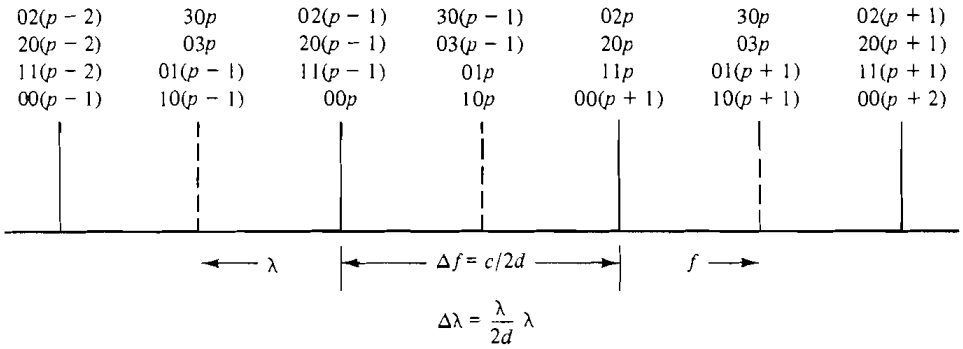


Figure 2.29: Resonance frequencies of the confocal Fabry-Perot resonator, [6], p. 128.

The odd modes are half way inbetween the longitudinal modes. Note, in contrast to the plan parallel Fabry Perot all mode frequencies are shifted by half of the free spectral range, $FSR = \frac{c}{2L}$, due to the Guoy-Phase-Shift.

# Bibliography


[1] Hecht and Zajac, "Optics," Addison and Wesley, Publishing Co., 1979.

[2] B.E.A. Saleh and M.C. Teich, "Fundamentals of Photonics," John Wiley and Sons, Inc., 1991.

[3] Bergmann and Schaefer, "Lehrbuch der Experimentalphysik: Opitk," 1993.

[4] H. Kogelnik and T. Li, "Laser Beams and Resonators," Appl. Opt. **5**, pp. 1550 – 1566 (1966).

[5] H. Kogelnik, E. P. Ippen, A. Dienes and C. V. Shank, "Astigmatically Compensated Cavities for CW Dye Lasers," IEEE J. Quantum Electron. **QE-8**, pp. 373 – 379 (1972).

[6] H. A. Haus, "Fields and Waves in Optoelectronics", Prentice Hall 1984.

[7] F. K. Kneubühl and M. W. Sigrist, "Laser," 3rd Edition, Teubner Verlag, Stuttgart (1991).

[8] A. E. Siegman, "Lasers," University Science Books, Mill Valley, California (1986).

[9] Optical Electronics, A. Yariv, Holt, Rinehart & Winston, New York, 1991.